Fat and Iron Quantification Using a Multi-Step Adaptive Fitting Approach with Multi-Echo GRE Imaging

Xiaodong Zhong[1], Marcel D. Nickel[2], Stephan A.R. Kannengiesser[2], Brian M. Dale[3], Berthold Kiefer[2], and Mustafa Bashir[4]
[1]MR R&D Collaborations, Siemens Healthcare, Atlanta, GA, United States, [2]MR Applications Development, Siemens AG, Healthcare Sector, Erlangen, Germany, [3]MR R&D Collaborations, Siemens Healthcare, Cary, NC, United States, [4]Division of Abdominal Imaging, Duke University Medical Center, Durham, NC, United States

Target Audience. MR physicists, clinical radiologists and abdominal MR radiologists.

Purpose. The rapid evaluation and quantification of hepatic fat and iron deposition is of great clinical interest. Among the chemical shift-based MRI methods for this purpose, techniques using complex signals usually utilize a priori information regarding field map smoothness (1,2), which is sensitive to phase variations or errors from other sources such as eddy currents and bipolar readout. Alternatively, utilizing only magnitude data from multi-echo signals to perform nonlinear fitting generates results insensitive to phase errors, but the known water-fat ambiguity cannot be easily resolved for fat percentage over 50% (3) and requires good initial value guesses for the fitting results to converge to correct solutions (4). Many other factors must be considered to quantify fat accurately, such as T_2* decay, T_1 bias, and multi-peak fat modeling. Additionally, R_2*/T_2* measurements are valuable indicators of hepatic iron deposition, and measuring water and fat R_2* separately may be informative. The purpose of this study was to develop a multi-step adaptive fitting approach for fat and iron quantification that accounts for all of the above factors, and to validate it with numeric synthesized data and a real in vivo case.

Theory. First, low flip angles are used for data acquisition, so that T_1 effects can be negligible (3). A three-step approach working for an acquisition with four or more flexible echo times is depicted in Fig. 1. Specifically, the dual-echo water fat separation method performed in Step 1 is described in (5). In Eqs. [1] and [2], c_n is the complex coefficient defined as $c_n = \sum w_i e^{j(2\pi\Delta f_i TE_n)}$ for a seven-peak fat model, where w_i and Δf_i are the weighting factor and the resonance frequency offset of the *i*th fat peak, respectively (6). Finally, the water, fat and their corresponding R_2* values are obtained, and fat percentage (FP) can be calculated.

Step 1:

Perform the dual-echo flexible-TE method to separate water (M_{w1}) and fat (M_{f1}), using two selected echoes (usually the first two echoes).

Step 2:

2.1 The magnitude values of the water and fat results from Step 1, i.e. $|M_{w1}|$ and $|M_{f1}|$, are used as initial guess values for M_{w2} and M_{f2}.

2.2 A constant value (e.g, 30 s^{-1}) is used as the initial guess value for R^*_{2eff}.

2.3 Perform Levenberg-Marquardt non-linear fitting based on Eq. [1]: $|S_n| = |(M_w + c_n M_f)\cdot e^{-R^*_{2eff}TE_n}|$ to calculate water (M_{w2}), fat (M_{f2}), and the effective R^*_{2eff}.

Step 3:

3.1 Use the water and fat results from Step 2, i.e. M_{w2} and M_{f2} as initial guess values for M_{w3} and M_{f3}

3.2 The effective R^*_{2eff} result from Step 2 is used as the initial guess value for both R^*_{2w} and R^*_{2f}.

3.3 Perform Levenberg-Marquardt non-linear fitting based on Eq. [2]: $|S_n| = |M_w \cdot e^{-R^*_{2w}TE_n} + c_n M_f \cdot e^{-R^*_{2f}TE_n}|$ to calculate water (M_{w3}), fat (M_{f3}), water R^*_{2w} and fat R^*_{2f}.

Fig. 1 Flow chart of the proposed approach.

Methods. This proposed approach was implemented as a reconstruction program online, which could also reconstruct data offline retrospectively.

In order to validate the accuracy of the proposed method, numeric phantoms were created in raw data format using a custom Matlab program (Mathworks, Natick, MA, United States) that can be fed to the reconstruction program, where in a 2D image nine circular regions with different FP and water/fat T_2* values were embedded in a big square region with gradually changing FP and water T_2*, and uniform fat T_2*, as shown in Fig. 2. Different acquisition features, including different field strengths, field maps, monopolar/bipolar readout, multi-echoes with different TEs, and noise levels, could be customized in the numeric phantom raw data.

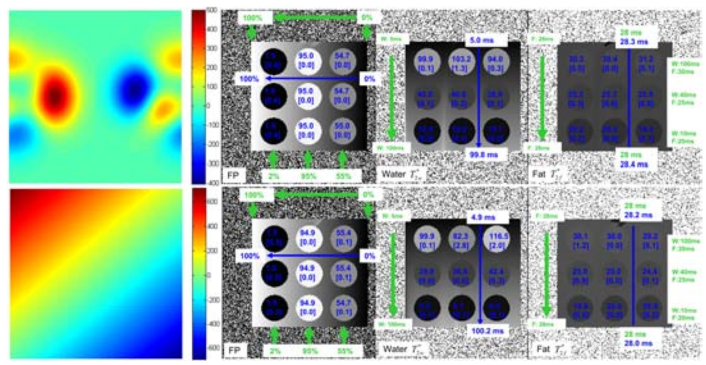

Fig. 2 The results of numeric phantom testing for two sets of conditions. The ground truth and measured values are showed in green and blue text, respectively. Top row: 3T, TE = 2.44, 4.91, 7.12, 9.45, 11.68, 13.98 ms, monopolar readout. Bottom row: 1.5T, TE = 0.87, 2.12, 3.5, 5, 6.5, 8 ms, bipolar readout. Left column: the corresponding ground truth B0 field map, in Hz. The fat spectrum is simulated with a seven-peak model (6).

In accordance with protocols approved by our local IRB, in vivo liver imaging data were acquired in patients on a 3 T MRI system (MAGNETOM Skyra, Siemens, Erlangen, Germany). A 3D volumetric interpolated breath hold examination (VIBE) (7) sequence was performed. Parameters included TR = 8.9 ms, flip angle = 4˚, pixel size = 1.4 – 1.6 mm, slice thickness = 4 mm, acquisition time = 20 s, first TE = 1.23 ms, and 6 echoes collected with ΔTE = 1.23 ms. As a reference standard for FP, a single-voxel high-speed T_2-corrected multiple-echo 1H-MRS sequence (HISTO) was also performed (8). The HISTO voxel was placed in liver region that was free of major hepatic vessels. The parameters included mixing time (TM) = 10 ms, TR = 3000 ms, TE = 12, 24, 36, 48 and 72 ms, 20 mm cubic voxel, bandwidth = 1200 Hz, sampling points = 1024, and acquisition time = 15 s. Values were measured offline with ImageJ (National Institutes of Health, Bethesda, MD) and presented as mean [standard deviation]. Using custom scripts written in Excel (Microsoft, Redmond, WA), the HISTO voxel position was registered on the 3D images.

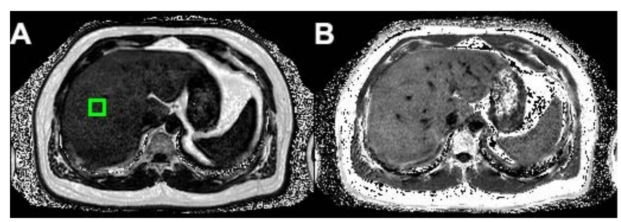

Fig. 3 Example FP (A) and water R_{2w}* (B) maps from one patient, respectively. The green box in (A) indicates the HISTO voxel position.

Results. Fig. 2 shows results of the proposed method for numeric phantoms in two sets of simulation conditions. Example FP and water R_{2w}* maps for one patient are shown in Fig. 3, where the mean FP was 16.0% and the mean water R_{2w}* value was 78.6 s^{-1} within the HISTO voxel position. HISTO measured that the FP of this same patient was 16.8%, and the water R_{2w} was 40.5 s^{-1}. Since HISTO measures R_2 (not R_2*), it could not directly be used to validate the R_2* results of the proposed method.

Discussion and Conclusions. In this work, a three-step adaptive fitting approach was proposed for fat and iron quantification. The numeric phantom validated the results measured by this approach with the ground truth, and showed that this approach is relatively insensitive to different field strengths, field inhomogeneity, monopolar/bipolar readout, and TE selections. An in vivo patient study showed consistency between the FP results measured with the proposed approach and a spectroscopy-based method, HISTO.

The step-wise initial guess estimation among these steps in the proposed method is critical for the Levenberg-Marquardt fitting to converge to the correct solutions in the multiple local minima situation, which is the nature of this non-convex optimization problem, and therefore overcome water-fat ambiguity for FP over 50%. TE selection strategies and the noise performance of the proposed approach remain to be investigated in further studies.

More patient results are presented in two additional abstracts submitted separately, including one reporting detailed correlation and statistic analysis against spectroscopy, and the other one reporting the pre- and post-contrast performance of FP and T2*/R2* measurement. Interested readers could refer to these two abstracts.

1. Chebrolu et al. Magn Reson Med 2010;63:849-857.
2. Hernando et al. Magn Reson Med 2010;63:79-90.
3. Bydder et al. Magn Reson Imaging 2008;26:347-359.
4. Yu et al. 17th ISMRM 2009;462.
5. Eggers et al. Magn Reson Med 2011;65:96-107.
6. Ren et al. J Lipid Res 2008;49:2055-2062.
7. Rofsky et al. Radiology 1999;212:876-884.
8. Pineda et al. Radiology 2009;252:568-576.